ISSN 1674-1056
http://cpb.iphy.ac.cn
http://iopscience.iop.org/cpb
中国物理 B
Chinese Physics
中国物理
Chinese Physics B

Performance study of aluminum shielded room for ultra-low-field magnetic resonance imaging based on SQUID: Simulations and experiments

Li Bo(李 波), Dong Hui(董 慧), Huang Xiao-Lei(黄小磊), Qiu Yang(邱阳), Tao Quan(陶泉), Zhu Jian-Ming(朱建明)
Citation: Chin. Phys. B . 2018, 27(2): 020701. **doi:** 10.1088/1674-1056/27/2/020701

Journal homepage: http://cpb.iphy.ac.cn; http://iopscience.iop.org/cpb

What follows is a list of articles you may be interested in

Modulation depth of series SQUIDs modified by Josephson junction area

Jie Liu(刘杰), He Gao(高鹤), Gang Li(李刚), Zheng Wei Li(李正伟), Kamal Ahmada, Zhang Ying Shan(张颖珊), Jian She Liu(刘建设), Wei Chen(陈炜)
Chin. Phys. B . 2017, 26(9): 098501. **doi:** 10.1088/1674-1056/26/9/098501

Bridge-free fabrication process for Al/AlO$_x$/Al Josephson junctions

Ke Zhang(张珂), Meng-Meng Li(李蒙蒙), Qiang Liu(刘强), Hai-Feng Yu(于海峰), Yang Yu(于扬)
Chin. Phys. B . 2017, 26(7): 078501. **doi:** 10.1088/1674-1056/26/7/078501

Technology demonstration of a novel poly-Si nanowire thin film transistor

Libin Liu(刘立滨), Renrong Liang(梁仁荣), Bolin Shan(单柏霖), Jun Xu(许军), Jing Wang(王敬)
Chin. Phys. B . 2016, 25(11): 118504. **doi:** 10.1088/1674-1056/25/11/118504

Low-T_c direct current superconducting quantum interference device magnetometer-based 36-channel magnetocardiography system in a magnetically shielded room

Qiu Yang, Li Hua, Zhang Shu-Lin, Wang Yong-Liang, Kong Xiang-Yan, Zhang Chao-Xiang, Zhang Yong-Sheng, Xu Xiao-Feng, Yang Kang, Xie Xiao-Ming
Chin. Phys. B . 2015, 24(7): 078501. **doi:** 10.1088/1674-1056/24/7/078501

Novel stability criteria for fuzzy Hopfield neural networks based on an improved homogeneous matrix polynomials technique

Feng Yi-Fu, Zhang Qing-Ling, Feng De-Zhi
Chin. Phys. B . 2012, 21(10): 100701. **doi:** 10.1088/1674-1056/21/10/100701

Performance study of aluminum shielded room for ultra-low-field magnetic resonance imaging based on SQUID: Simulations and experiments*

Bo Li(李波)[1,2,3], Hui Dong(董慧)[2,3], Xiao-Lei Huang(黄小磊)[2,3,4], Yang Qiu(邱阳)[1,2,3], Quan Tao(陶泉)[2,3], and Jian-Ming Zhu(朱建明)[1,†]

[1] *China Jiliang University, Hangzhou* 310018, *China*
[2] *State Key Laboratory of Functional Materials for Informatics, Shanghai Institute of Microsystem and Information Technology (SIMIT), Chinese Academy of Sciences (CAS), Shanghai* 200050, *China*
[3] *CAS Center for ExcelleNce in Superconducting Electronics (CENSE), Shanghai* 200050, *China*
[4] *University of Chinese Academy of Sciences, Beijing* 100049, *China*

(Received 3 May 2017; revised manuscript received 20 November 2017; published online 5 January 2018)

The aluminum shielded room has been an important part of ultra-low-field magnetic resonance imaging (ULF MRI) based on the superconducting quantum interference device (SQUID). The shielded room is effective to attenuate the external radio-frequency field and keep the extremely sensitive detector, SQUID, working properly. A high-performance shielded room can increase the signal-to-noise ratio (SNR) and improve image quality. In this study, a circular coil with a diameter of 50 cm and a square coil with a side length of 2.0 m was used to simulate the magnetic fields from the nearby electric apparatuses and the distant environmental noise sources. The shielding effectivenesses (SE) of the shielded room with different thicknesses of aluminum sheets were calculated and simulated. A room using 6-mm-thick aluminum plates with a dimension of 1.5 m×1.5 m×2.0 m was then constructed. The SE was experimentally measured by using three-axis SQUID magnetometers, with tranisent magnetic field induced in the aluminum plates by the strong pre-polarization pulses. The results of the measured SE agreed with that from the simulation. In addition, the introduction of a 0.5-mm gap caused the obvious reduction of SE indicating the importance of door design. The nuclear magnetic resonance (NMR) signals of water at 5.9 kHz were measured in free space and in a shielded room, and the SNR was improved from 3 to 15. The simulation and experimental results will help us design an aluminum shielded room which satisfies the requirements for future ULF human brain imaging. Finally, the cancellation technique of the transient eddy current was tried, the simulation of the cancellation technique will lead us to finding an appropriate way to suppress the eddy current fields.

Keywords: shielding effectiveness, aluminum shielded room, eddy current cancellation technique, superconducting quantum interference device, ultra-low-field magnetic resonance imaging

PACS: 07.55.Nk, 85.25.Dq, 87.61.–c **DOI:** 10.1088/1674-1056/27/2/020701

1. Introduction

Ultra-low-field magnetic resonance imaging (ULF MRI), working in the magnetic fields in the order of tens to hunderds of micro-tesla (μT), is becoming increasingly popular. Compared with traditional high-field MRI, ULF MRI has several significant advantages,[1] for example, capable of imaging in the presence of metallic objects,[2] contrast enhancement between cancerous and benign tissues,[3] simultaneous functional and anatomical imaging of the human brain with magnetoencephalography (MEG) and MRI,[4,5] etc. Practically, the acquisition of high quality images with ULF MRI has been challenging. Two methods have been commonly applied to improve the signal-to-noise ratio (SNR). The first one is the pre-polarization technique.[6] The signal amplitude can be increased by using a pulsed prepolarization field (B_p) much stronger than the static field (B_0), which determines the signal frequency, so that the initial nuclear magnetization is now proportional to B_p and independent of B_0.[7] The second solution is to use superconducting quantum interference devices (SQUIDs) as the detecting sensors. SQUID is a flux sensor with extremely low intrinsic noise (only a few fT/Hz$^{1/2}$). As a result, it is a promising choice for ULF NMR & MRI applications. Because the B_0 field of ULF MRI is on the order of Earth's field, the influence of the environment magnetic field can be significant. Low-frequency fluctuations,[8–10] typically (< 10 Hz) and the static gradient[11,12] of the environmental magnetic field can degrade the SNR, and cannot be shielded by aluminum sheets. These challenges were successfully overcome by using the active compensation[13] and the full-tensor gradient compensation.[11] Besides, the strong white noise and power-line harmonics affect the signal in the MRI signal band, so we setup the entire system in an aluminum shielded room.

Shielding of ULF MRI systems can be realized by using two different types of materials: high magnetic perme-

*Project supported in part by the Strategic Priority Research Program (B) of the Chinese Academy of Sciences (Grant No. XDB04020200) and in part by the National Natural Science Foundation of China (Grant No. 11204339).
†Corresponding author. E-mail: drzhulab@gmail.com
© 2018 Chinese Physical Society and IOP Publishing Ltd

ability materials or high electrical conductivity materials.[14] Usually, a magnetically shielded room can use both materials, but a conductively shielded room only uses the high conductivity materials such as aluminum.[15] Some groups who focused particularly on hybrid anatomical and functional brain imaging, i.e., the combination of MRI and MEG, developed their systems in magnetically shielded rooms. In contrast, the UC Berkeley group only used aluminum sheets to construct a shielded room for the structural brain imaging and relaxation-time-contrast (T1-contrast) imaging.[16–18] In this design, the sizes of aluminum sheets were reduced and the neighboring plates were weakly connected to reduce the time constants of eddy currents in the sheets, which were induced by the strong B_p pulse. This design may provide adequate shielding for the ULF MRI system. A shielded room with 3-mm-thick aluminum sheets was constructed in our laboratory similar to the design of the UC Berkeley group.[16–18] Since our laboratory sits in a downtown location and the magnetic field in the laboratory is heavily polluted by the ambient magnetic field noise, the shielding factors of this 3-mm-thick shielded room may not meet the requirements of ULF MRI.

In the current study, the shielding factors of aluminum shielded rooms with different thicknesses were compared by theoretical calculation and simulation. A new 6-mm-thick aluminum shielded room with a dimension of 1.5 m×1.5 m×2.0 m was designed and constructed for *in-vivo* tissue imaging. Three-axis SQUID magnetometers were used to measure the pratical SE of the shielded room in the static and fluctuated field to examine the shielding effects on the nearby electric apparatus and the distant environmental magnetic field noise sources, respectively. We showed the measured noise, and the proton nuclear magnetic resonance (NMR) signals of water in free space and in the shielded room. Finally, we proposed a transient residual field cancellation technique and performed the simulation demonstrated.

2. ULF MRI system

Our ULF MRI setup shown in Fig. 1 consists of the MRI coil system and a commercial liquid helium (LHe) Dewar, which provides the cryogenic working environment for the low-T_c SQUID sensor. The coil system includes the coil pairs

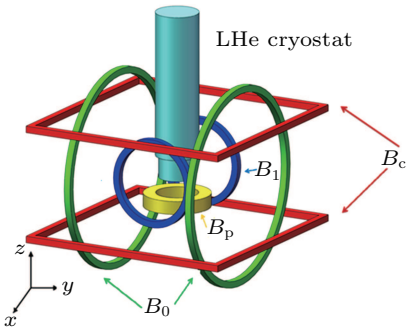


Fig. 1. (color online) Schematic diagram of the ULF MRI system. The imaging gradient coil pairs are not drawn for simplicity.

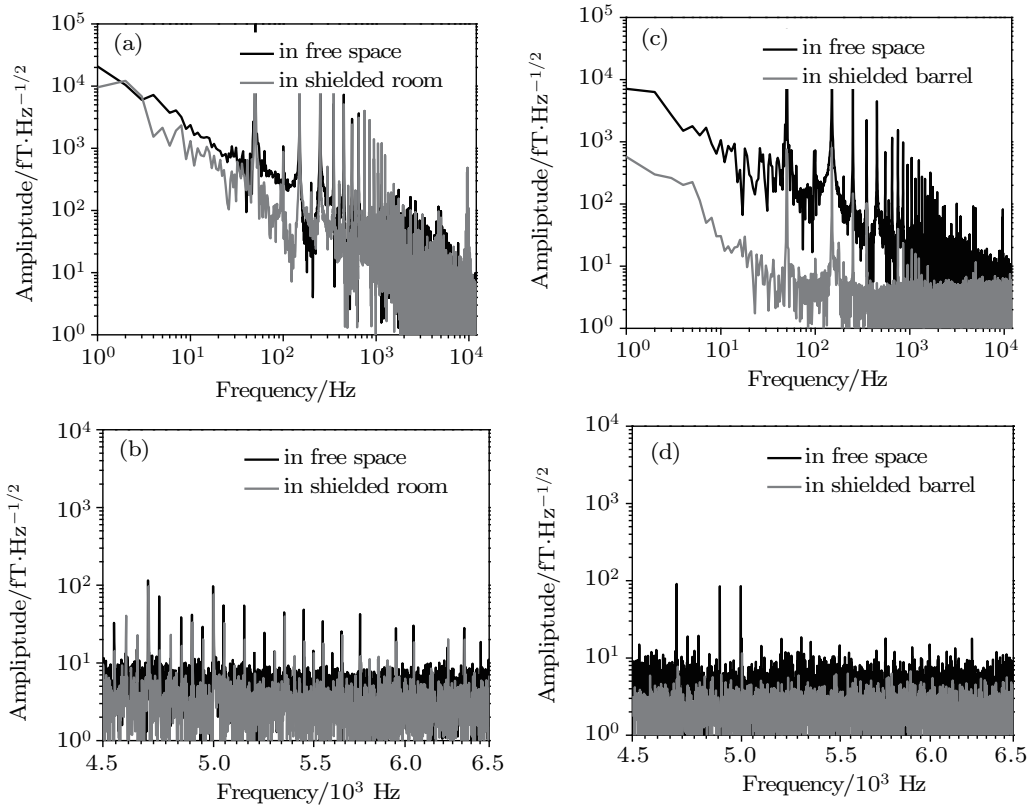


Fig. 2. (a) Broadband noise specturm, and (b) noise in image bandwidth measured by the second-order SQUID gradiometer in the free space (black), and in the 3-mm-thick shielded room (gray). Panels (c) and (d) are the broadband noise and image-band noise spectra measured in the free space (black), and in the magnetically shielded barrel (gray).

to generate the B_0 field, the B_1 excitation pulse, and the B_c field to cancel the vertical component of the Earth's field, respectively. The strong B_p pulse is generated by a water-cooled copper coil. A home-made wire-wound second-order SQUID gradiometer was used to acquire the MRI images. The diameter and the baseline of the gradiometer are 22 mm and 50 mm, respectively.

Typical noise spectra measured by the second-order SQUID gradiometer are shown in Fig. 2. Strong power-line harmonics noise peaks below 10 kHz can be seen in Fig. 2(a). In the imaging bandwidth (Fig. 2(b)), the peak amplitude of 50 Hz harmonics reaches up to 40 fT/Hz$^{1/2}$. Those peaks reduce the imaging quality and narrow the signal bandwidth.[8–11] In addition, the 3-mm-thick shielded room attenuates white noise by only 2.5 dB. For comparsion purposes, the system noise, dominated by the Dewar noise and the sensor noise, was measured in a magnetically shielded barrel, constructed by 5-layer μ-metal (Figs. 2(c) and 2(d)). The Dewar noise and the sensor noise were 3 fT/Hz$^{1/2}$, respectively. The system white noise was measured to be about 5 fT/Hz$^{1/2}$. Considering the harsh magnetic field environment in the laboratory, a new shielded room with better shielding performance was designed and constructed. Our goal was that the new shielded room can attenuate the white noise by 6 dB, or reduce the noise to be below the system noise. For the purpose of *ex-vivo* tissue imaging, the ULF MRI coil system was designed as compact, such that the size of the shielded room can be reduced with lower cost. In the following sections, the design, simulation, and the measurement of the performance of the shielded room are discussed.

3. Theoretical calculation and simulation of the shielding factors with different thickness of aluminum

3.1. Conductive shielding theory

Eddy current shielding takes place when the plane electromagnetic waves enter a conductor. The induced eddy current will produce a magnetic field opposite to the direction of the time-varying external magnetic fields, and the shielded room is used to attenuate external environmental noises. The magnetic field will be damped exponentially with the penetration or skin depth δ given by[19]

$$\delta = \sqrt{(\rho/\pi\mu_0\mu_r f)}, \tag{1}$$

where ρ is the resistivity, μ_0 the permeability of a vacuum, μ_r the relative permeability, and f the frequency of the time-varying electromagnetic wave.

At low frequencies, when the thickness of the high electrical conductivity sheets t is less than δ, the surface eddy current shielding dominates. For a model of a rectangular tube, the shielding factor S is given by[15]

$$S = \sqrt{[1+(\omega\tau)]^2}, \tag{2}$$

where

$$\omega\tau = \frac{\pi\mu_0 f wht}{(w+h)\rho} = wht/(w+h)\delta^2, \tag{3}$$

and, w, h, and t, are the width, height, and thickness of the tube, respectively. $\omega = 2\pi f$ corresponds to the angular frequency, and τ is the time constant of the rectangular tube in response to the external magnetic field.

At high frequencies that lead to $t < \delta$, the exponential decay of the field inside the conductor should be considered and the shielding factor can be written as[19]

$$S = \left[\left(\frac{1}{4\sqrt{2}}\right) e^{t/\tau}\left(\frac{2wh}{(w+h)\delta}\right)\right]. \tag{4}$$

According to Eqs. (2) and (4), the theoretical shielding effectiveness (SE) SE $= 20\log(S)$ can be calculated. Figure 3(a) shows that the calculated SE is a function of frequency for different thicknesses of aluminum sheets ranging from 3 mm to 7 mm. The SE at the signal frequency of 5.5 kHz may reach 94 dB when the aluminum thickness is 6 mm.

3.2. Simulation of the shielding effectiveness (SE)

SE depends on the aluminum sheets, as can be seen from Fig. 3(a). Several published studies[19–21] have shown that the measured SE is lower than the theoretical values as calculated by Eqs. (2) and (4). There is no exact theory or formula which can be used for calculation of the practical SE at frequencies above 10 Hz.[19] In order to gain an actual reference, we simulate the new shielded room using a commerical finite element analysis software. The simulation can be divided into three steps: pre-processing, calculation, and post-processing. In the pre-processing step, the modeling is done according to the dimesions of the shielded room and the size of our system setup. The shielded room dimensions are 1.5 m×1.5 m×2.0 m, and the type of aluminum alloy is 6061. Then we mesh the model and calculate the magnetic fields at the sample position. In post-processing, the shielding effectiveness SE $= 20\log(\boldsymbol{B}_f/\boldsymbol{B})$ is calculated with the magnetic field $\boldsymbol{B}_f$ in the free space without shielding and the magnetic field B in the shielded room. The simulated results are shown in Fig. 3(b). The SE increased with the increase of the sheet thickness from 3 mm to 7 mm, which agreed with the theoretically calculated results. Note that, at the frequency of 5.5 kHz, the SE of the room is about 67 dB when the thickness of Al plate is 6 mm. The comparison between the calculation and simulation results showed that the shielding performance in the kHz range cannot be calculated with simple and accurate formula, which is in agreement with the conclusion from Ref. [20]. Considering the gaps existing between

the plates and the door, the simulated SE of the room is usually better than the actual values. Consequently, a model of the new shielded room with a 0.5-mm gap between one plate and the door was developed, referring to the seams existing in the 3-mm-thick shielded room. The simulated results are shown in Fig. 3(c). The SE agreed with the results in Figs. 3(a) and 3(b). However, the SE at 5.5 kHz reduced from 67 dB to only 26.4 dB when the aluminum thickness is 6 mm, and the SE at 5.5 kHz is 25.5 dB when the thickness is 5 mm. Our goal for the SE of the new shielded room is 3.5 dB higher than the 3-mm-thick shielded room (23 dB). After overall consideration of the room weight and cost, aluminum sheets with a thickness of 6-mm were chosen to construct the shielded room.

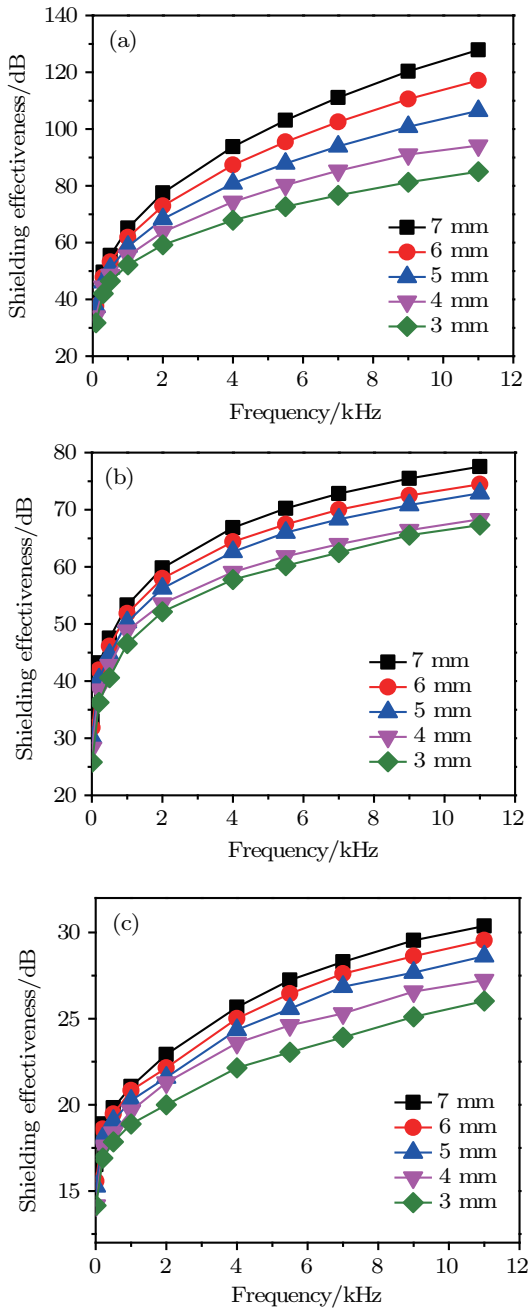


Fig. 3. (color online) Theoretically calculated (a) and simulated (b) SE as a function of frequency for different thicknesses of aluminum sheets. (c) Simulated results with a 0.5-mm gap between one plate and the door.

4. Experiments in the 6-mm-thick shielded room

Figure 4(a) shows the schematic diagram of the system. The shielded room was built using the same dimensions as the simulated model. The 6-mm-thick plates were tightly bolted to the wooden supporting frame using stainless steel bolts. The door was suspended on four stainless steel hinges. The conducting fabric was attached to the outer frame of the door to prevent electromagnetic interference (EMI) from the external environment.

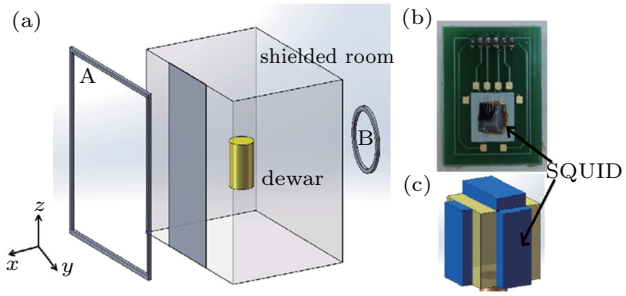


Fig. 4. (color online) (a) Schematic diagram of the system. Coils A and B represent the square coil and the circular coil, respectively. The three-axis SQUID magnetometers are placed in the Dewar. The rectangular cylinder is the 1.5 m×1.5 m×2.0 m shielded room, and the shaded rectangle is the door. (b) The SQUID chip with a size of 4 mm×4 mm. The inductance of the SQUID chips is 190 pH. (c) The frame of three-axis magnetometer.

Generally speaking, two noise sources may influence the performance of our system. The first one is the environmental magnetic field noise. Usually the environmental noise is produced by distant noise sources and may be considered as a time-varying uniform field in the system region. The other noise source is the nearby electric apparatus, which produces a non-uniform field near the sample. In order to examine the performance of our newly designed shielded room for isolating the time-varying uniform components and fluctuated magnetic fields, a large square coil A with 2-m length (the number of turns $N = 50$) was used to produce a time-varying uniform field (Fig. 4(a)). The coil A was placed in front of the door with its axis perpendicular to the door, because the shielding effect of the shielded room was limited by the door gaps. In addition, a small circular coil B with 50-cm diameter ($N = 12$ turns) was located behind the room to simulate the field noise generated by the system electric apparatus. The coil B was used to optimize the distance to place the system equipment. For both coils the SE of the room was measured with different distances between the room center and the coil. The distances are 1.6 m, 1.75 m, 1.9 m, 2.1 m, 2.25 m, and 2.4 m, respectively. At 2.25 m, the SE at different frequencies ranging from 90 Hz to 11 kHz was obtained by feeding the current to the coils using a Kikusui Bipolar Power Supply (PBZ 20-20).

Home-made three-axis SQUID magnetometers (as shown in Figs. 4(b) and 4(c)) were employed to measure the horizontal components B_x, B_y, and the perpendicular component B_z of the environmental magnetic field, with the total magnetic field

calculated from $\boldsymbol{B} = \sqrt{(B_x^2 + B_y^2 + B_z^2)}$ at the positions where the specimens were placed. Similarly, the magnetic field $\boldsymbol{B}_\mathrm{f}$ in the free space without shielding was measured. The shielding factor can be calculated by $S = \boldsymbol{B}_\mathrm{f}/\boldsymbol{B}$. The results of SE measurement are shown in Fig. 5.

For the effects of homogenous distant magnetic noise (Fig. 5(a)), the comparision among the results from the theoretical calculation, the simulation with and without the 0.5 mm gap between one plate and the door, as well as the measurements, was found that the latter three cases showed quite similar trends with the increase of the frequency. In contrast, the SE of the theoretical curve rises quicker than the other three curves when the frequency increases. The measured SE is slightly better than the simulation with a 0.5-mm gap between one plate and the door, because in the actual shielded room, the narrow slits between the plates are covered by aluminum foil tapes and the gaps between the plates and the door were covered by conducting fabrics.

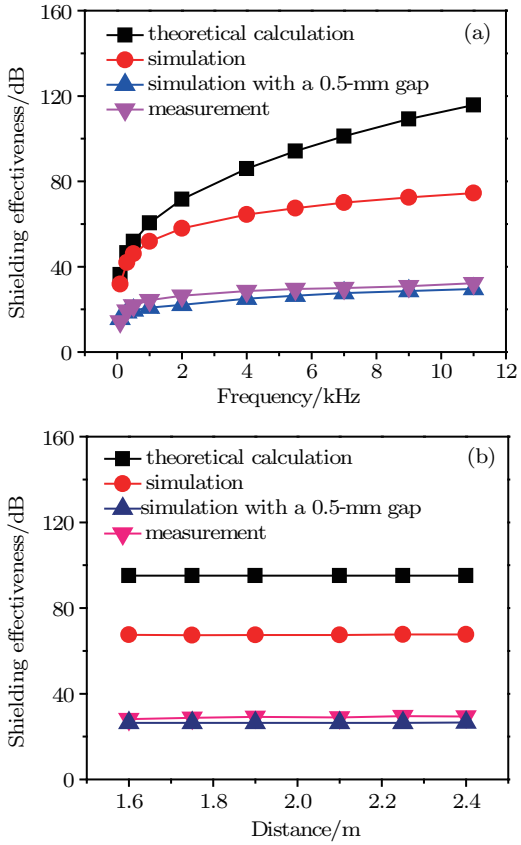


Fig. 5. (color online) (a) Shielding effectiveness as a function of frequency with coil A 2.25 m away from the sample position for theoretical calculation (black square), the simulation without (red circle) and with a 0.5-mm gap (blue triangle), and the measured results (pink inverted triangle). (b) Shielding effectiveness at 5.5 kHz for different distances.

For the case of coil B, as shown in Fig. 6(a), similar relationships exist among the results from calculation, simulation, and measurements as shown in Fig. 5(a). Considering that the seams behind the room are narrower than those in the front of the room, a gap of 0.1 mm between Al alloy plates was set in the simulation. The measured SE is very close to that of the simulation with a 0.1-mm gap. Note that the measured SE for coil B is higher than the value for coil A, but their simulation results with no gap are almost the same. For example, the SE for coil B is about 40 dB at 5.5 kHz, 10 dB higher than that for coil A. This difference is due to the leakage through holes and gaps near the door, which is in the vicinity of coil A. Therefore, simulation with considering the seams may be the optimal method to improve the design of the shielded room.

The results of SE, as a function of coil distance, were also measured as shown in Fig. 5(b) and Fig. 6(b). The discrepancy between the two figures indicates that the SE for coil B slightly changes with the distances, and the SE reduces from 44 dB to 39 dB. It is because when the small exciting coil is close to one of the walls of the room, the shielding currents are induced only in that wall but not in the other walls.[14] From the experiments, we concluded that the electric apparatus should be as far away from the room as possible, at least as far as the length of the shielded room.

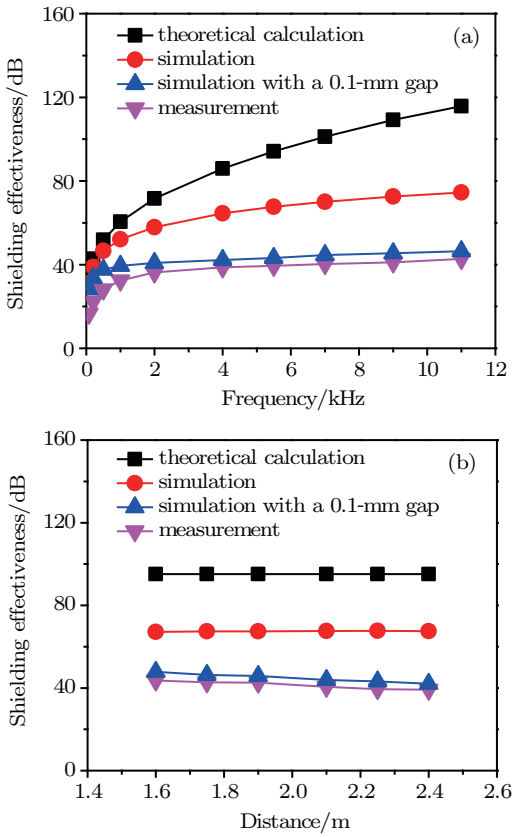


Fig. 6. (color online) (a) Shielding effectiveness as a function of frequency with coil B 2.25 m away from the sample position for theoretical calculation (black square), the simulation without (red circle) and with a 0.5-mm gap (blue triangle), and the measured results (pink inverted triangle). (b) Shielding effectiveness at 5.5 kHz for different distances.

The magnetic field noise in the newly designed shielded room and in the free space of the laboratory were then measured with the second-order gradiometer. The noise spectra are shown in Fig. 7. The power-line harmonics in the newly designed shielded room is effectively eliminated in the imaging

frequency bandwidth from 5 kHz to 6 kHz, and the white noise level was reduced from 20 fT/Hz$^{1/2}$ to 10 fT/Hz$^{1/2}$. The new shielded room can attenuate the white noise nearly by half, which meets the design requirements.

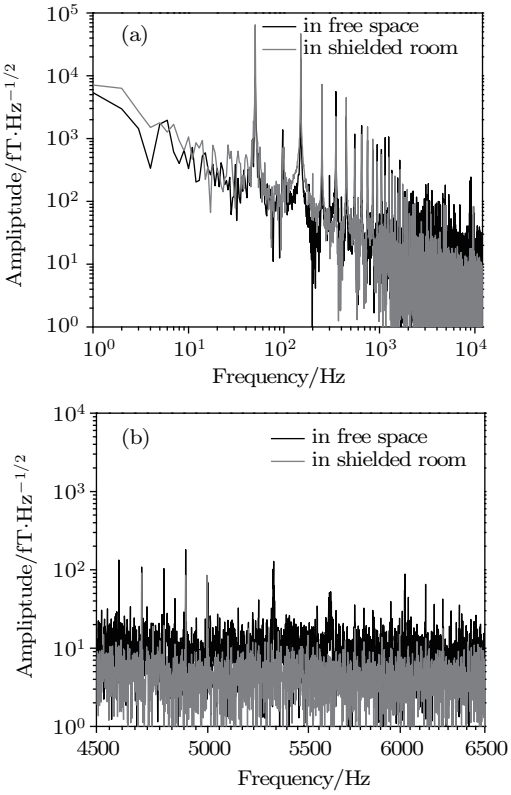


Fig. 7. (a) Broadband noise spectrum and (b) noise in image frequency bandwidth measured by the second-order SQUID gradiometer in the free space (black), and in the shielded room (gray).

Figures 8(a) and 8(b) show the proton NMR signals of water at 5.9 kHz in free space and in the shielded room, respectively. During the measurement, the B_p coil has to be placed 130 mm away from the Dewar due to the interference from the external radio-frequency fields, the B_p field at the sample is only about 10 mT. The white noise can reach up to 30 fT/Hz$^{1/2}$, and the SNR is less than 3. In contrast, the radio-frequency field can be attenuated effectively in the 6-mm-thick shielded room. Consequently, the distance between the B_p coil with Dewar is shortened to be about 90 mm and the B_p field reaches 20 mT at the sample position. The white noise is attenuated to 10 fT/Hz$^{1/2}$. Because the strong B_p pulse induces transient currents in the walls of the surrounding conductive shielded room, we have to wait about 90 ms until the SQUID electronics can be locked, which loses the very initial part of the signal. Therefore, the SNR reaches to 15 in the shielded room.

The SE and the SNR of the 6-mm-thick shielded room satisfy the design requirements for ULF MRI experiments. When the system was upgraded for *ex vivo* tissue studies using a large, water-cooled polarizing coil, the transient magnetic fields produced by the induced eddy currents in aluminum plates would interfere with the measurements. The eddy current fields will deteriorate the homogeneity of B_0 and the linearity of the imaging gradient fields. In addition, the strong eddy current fields will exceed the dynamic range of the SQUID readout electronics and prolong the system dead time. The decay time of the eddy-current induced transient fields is determined by the response time constant[12]

$$\tau = \mu_0 \frac{\sigma wht}{2(w+h)}, \tag{5}$$

where σ is the conductivity of aluminum.

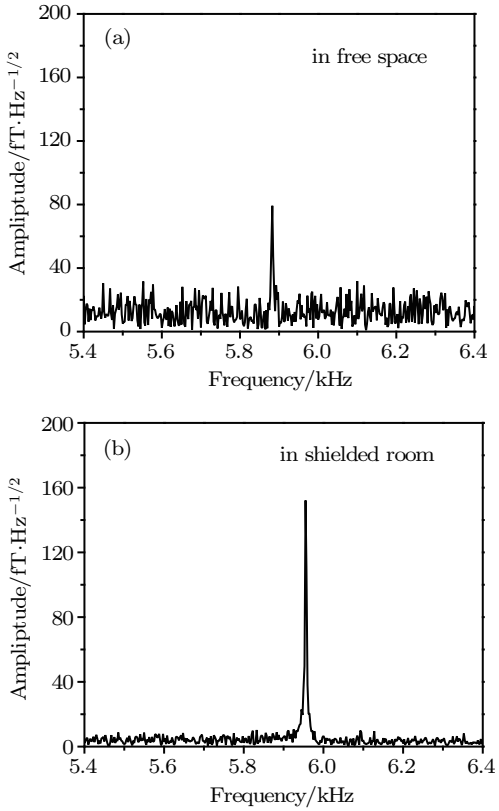


Fig. 8. NMR signals at 5.9 kHz (a) in the free space, and (b) in the 6-mm-thick shielded room.

By measuring the eddy current field response to square wave, the measured response time of the newly designed shielded room is about 23 ms. The decay of eddy current field could last more than 100 ms, and thus an effective eddy current cancellation technique is needed for future ULF MRI experiments. Finite analysis software was used to simulate how to cancel the influence of the transient residual fields, as shown in Fig. 9(a) for the model of our cancellation technique. Two axial perpendicular Helmholtz coils were designed to neutralize magnetic fields at the sample position generated on the aluminum plates by the B_p coil. The distance between the center of the upper part of the Helmholtz coil and the center of the shielded room is 0.5 m. The radius of the coil is 0.5 m ($N = 140$ turns). The lower part of the coils are similar to the upper part, only the position is the opposite. The results are shown in Fig. 9(b). The response time constant in this simulated model was 27 ms, which agrees with the experimental results. When the B_p field was 53 mT, the transient residual

field at the sample position can be reduced from 215 μT to 15 μT. The transient field can be further attenuated to 5 μT in 50 ms after the cutoff of B_p current. The simulated results showed that the cancellation model satisfied our requirements for ULF MRI.

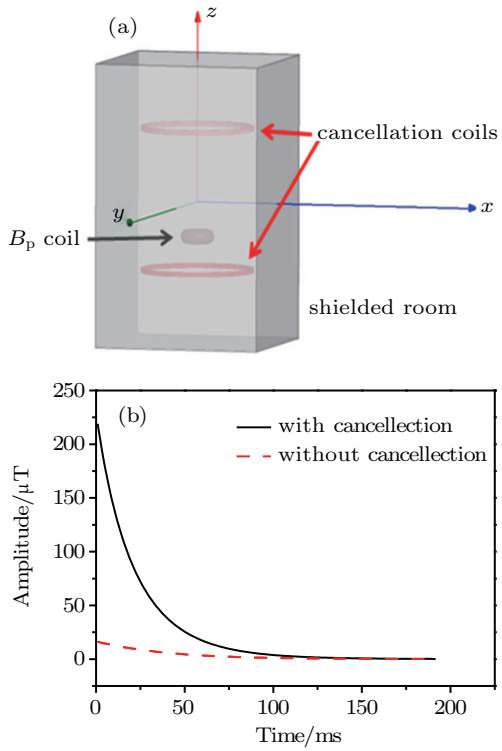


Fig. 9. (color online) (a) The sketch of the simulated cancellation system, (b) the transient residual field with (red dashed line) and without (black solid line).

5. Conclusions and outlook

In this paper, the SE of the aluminum shielded room was compared among the results of experimental measurements, and the calculation and simulation results. A shielded room with 6-mm-thick aluminum plates was designed and constructed. The measured SE and the noise spectra demonstrated that this shielded room meets the preliminary requirements for attenuating the white noise as well as the power-line harmonics in the imaging frequency bandwidth. The SNR of the NMR signal was improved by a factor of 5 in the newly designed shielded room. Finally, the finite element analysis was used to verify the proposed cancellation scheme and obtain the relevant parameters. To further validate our analysis and the design of shielded room, more experimental results are needed to prove this eddy current cancellation technique, particularly, *ex vivo* tissue images will be acquired.

References

[1] Vrba J, Nenonen J and Trahms L 2006 *Biomagnetism, The SQUID Handbook Volume II: Applications of SQUIDs and SQUID Systems*, ed. Clake J and Braginski A I (Weinheim: Wiley-VCH) pp. 269–390
[2] Mößle M, Han S I, Myers W, Lee S K, Kelso K, Hatridge M, Pines A and Clarke J 2006 *J. Magn. Reson.* **179** 146
[3] Lee S K Mößle M Myers W Kelso K Trabesinger A H, Pines A and Clarke J 2005 *Magn. Reson. Med.* **53** 9
[4] Zotev V S, Matlashov A N, Volegov P L, Savukov I M, Espy M A, Mosher J C, Gomez J J and Kraus R H 2008 *J. Magn. Reson.* **194** 115
[5] Vesanen P T *et al.* 2013 *Magn. Reson. Med.* **69** 1795
[6] Macovski A and Conolly S 1993 *Magn. Reson. Med.* **30** 221
[7] Myers W, Slichter D, Hatridge M, Busch S, Mößle M, Robert McDermott, Trabesinger A and Clarke J 2007 *J. Magn. Reson.* **186** 182
[8] Qiu L Q, Liu C, Dong H, Xu L, Zhang Y, Krause H J, Xie X M and Offenhäusser A 2012 *Chin. Phys. Lett.* **29** 107601
[9] Qiu L Q, Zhang Y, Krause H J, Braginski A I and Offenhäusser A 2009 *J. Magn. Reson.* **196** 101
[10] Jin Y R, Wang N, Li S, Tian Y, Ren Y F, Wu Y F, Deng H, Chen Y F, Li J, Tian H Y, Chen G H and Zheng D N 2011 *IEEE Trans. Appl. Supercond.* **21** 2962
[11] Dong H, Qiu L Q, Shi W, Chang B L, Qiu Y, Xu L, Liu C, Zhang Y, Krause H J, Offenh?usser A and Xie X M 2013 *Appl. Phys. Lett.* **102** 102602
[12] Jiang F Y, Wang N, Jin Y R, Deng H, Tian Y, Lang P L, Li J, Chen Y F and Zheng D N 2013 *Chin. Phys. B* **22** 047401
[13] Qiu L Q, Liu C, Dong H, Xu L, Zhang Y, Krause H J and Xie X M 2012 *Phys. Procedia* **36** 388
[14] Stroink G, Blackford B, Brown B and Horacek M 1981 *Rev. Sci. Instrum.* **52** 463
[15] Zimmerman J E 1977 *J. Appl. Phys.* **48** 702
[16] Zevenhoven K C J, Busch S, Hatridge M, Öisjöen F, llmoniemi R J and Clarke J 2014 *J. Appl. Phys.* **115** 103902
[17] Zevenhoven K J, Dong H, Ilmoniemi R J and Clarke J 2015 *Appl. Phys. Lett.* **106** 034101
[18] Hatridge M J 2010 "SQUID magnetometry from nanometer to centimeter length scales", Ph. D. thesis (University of California: Berkeley)
[19] Ma Y P and Wikswo J P Jr 1991 *Rev. Sci. Instrum.* **62** 2654
[20] Schweizer F 1962 *J. Appl. Phys.* **33** 1001
[21] Sullivan G W, Lewis P S, George J S and Flynn E R 1989 *Rev. Sci. Instrum.* **60** 765
[22] Aden A L and Kerker M 1951 *J. Appl. Phys.* **22** 1242